Journal of The Electrochemical Society, **161** (12) F1133-F1139 (2014)
0013-4651/2014/161(12)/F1133/7/$31.00 © The Electrochemical Society

Sulfur Deposition and Poisoning of $La_{0.6}Sr_{0.4}Co_{0.2}Fe_{0.8}O_{3-\delta}$ Cathode Materials of Solid Oxide Fuel Cells

Cheng Cheng Wang, Kongfa Chen, and San Ping Jiang[z]

Fuels and Energy Technology Institute & Department of Chemical Engineering, Curtin University, Perth, WA 6102, Australia

Sulfur in the air stream is one of the major contaminants affecting the performance stability of cathodes of solid oxide fuel cells (SOFCs) such as $La_{0.6}Sr_{0.4}Co_{0.2}Fe_{0.8}O_{3-\delta}$ (LSCF) perovskite. Here sulfur deposition and poisoning was investigated on LSCF bar samples in the presence of 20 ppm SO_2 and temperature range of 400–900°C, using scanning electron microscopy, confocal laser Raman spectroscopy and electrical conductivity relaxation (ECR) methods. Sulfur (SO_2) reacts with LSCF, primarily forming $SrSO_4$ at high temperatures (i.e., $\geq$ 700°C) and SrS at low temperatures (i.e. <700°C). Surface segregated SrO plays an important role in the sulfur deposition. The most important observation of this study is that sulfur deposition shows a distinct volcano-type dependency on the heat-treatment temperature and is most pronounced at temperatures around 700°C, indicating that the reaction rate between the segregated SrO and SO_2 is highest at ~700°C. The ECR results indicate that the surface exchange coefficient of LSCF after the exposure to 20 ppm SO_2 at 700, 800 and 900°C for 48 h is two orders of magnitude lower than that of the sample tested in the absence of SO_2, indicating that sulfur poisoning deteriorates significantly the surface exchange and diffusion processes for the O_2 reduction reaction on LSCF electrodes.
 [DOI: 10.1149/2.0041412jes]

Manuscript submitted July 10, 2014; revised manuscript received July 30, 2014. Published August 8, 2014.

Fuel cells are electrochemical conversion devices to effectively convert chemical energy of fuels to electricity with high efficiency and low greenhouse gas emission. Among all types of fuel cells, solid oxide fuel cells (SOFCs) operating at intermediate temperatures of 500–800°C offer an attractive option that is much more fuel flexible than low temperature fuel cells such as proton exchange membrane fuel cells (PEMFCs) and is suitable for a wide range of applications. However, a major issue over a 5 year life-time of a SOFC system is the gradual degradation and deactivation of the cathodes by contaminants such as chromium, sulfur and boron which can be either in the air stream or from the volatile species of cell components, such as metallic interconnect, sealant and manifold.[1–7]

Sulfur is one of the major contaminants in SOFCs. For example, one of the major challenges for the direct use of hydrocarbon fuels in SOFCs is the poisoning of Ni-based anodes by sulfur existed as impurities in readily available hydrocarbon fuels.[8,9] The presence of H_2S degrades the performance of the Ni-based anodes such as Ni/Y_2O_3-ZrO_2 (Ni/YSZ) and Ni/Gd_2O_3-CeO_2 (Ni/GDC) cermet anodes.[10–12] Sulfur in the air stream can also affect significantly the performance and durability of SOFCs.[13–16] One possible source of sulfur contamination is the presence of a trace amount of SO*x* in air, which could be accumulated by reacting with the cathode in the vicinity of the air entrance of cells. In contrast with the extensive studies on the mechanism and kinetics of the deposition and poisoning of sulfur on the anodes of SOFCs,[17] much less attention has been paid on the sulfur deposition and poisoning on the cathode materials. Understanding the sulfur deposition and poisoning mechanism is critical to develop contaminant-tolerant and durable cathodes for SOFCs.

Xiong et al. studied the polarization behavior of $(La_{0.85}Sr_{0.15})_{0.95}MnO_3$ (LSM) and $Sm_{0.5}Sr_{0.5}CoO_3$ (SSC) cathodes after the heat-treatment of the electrodes to 100 ppm SO_2 at 800°C and found that the performance of SSC declined rapidly while LSM was more stable in SO_2-contained air.[15] The significant difference in the polarization performance of SSC and LSM in SO_2-contained air for the O_2 reduction reaction has been explained by the difference in the activity of SrO in the LSM and SSC perovskites. Liu et al.[13] showed that the performance of cells with $La_{0.6}Sr_{0.4}Co_{0.2}Fe_{0.8}O_{3-\delta}$ (LSCF) electrode becomes unstable in the presence of 1 ppm SO_2 and drops significantly when the SO_2 concentration increased to 20 ppm. The performance degradation is most likely due the poisoning of SO_2 and the formation of $SrSO_4$. Sitte et al measured the surface exchange kinetics of a dense $La_{0.6}Sr_{0.4}CoO_{3-\delta}$ sample at 700°C and observed the decreases in the surface exchange coefficient, k_{chem} in the presence of a small amount of sulfur (ppb).[18] Ishihara's group[19] reported that the degradation of LSCF is accelerated at low partial pressure of O_2 in the presence of sulfur and the degradation is considered to be caused by the Sr segregation and the subsequent formation of $SrSO_4$. On the other hand, Wang et al.[20] studied the polarization performance behavior of LSCF in the presence of 0.1 ppm SO_2 and two-stages of performance degradation were found. A degradation mechanism based on the occupation of SO_2 in the oxide ion vacancies and subsequent formation of SO_3^{2-} and $SrSO_4$ was proposed for the irreversible poisoning effect of SO_2. However, there appears no consensus on the mechanism and kinetics of the deposition and poisoning of sulfur on SOFC cathodes such as LSCF.

In this study, the deposition and poisoning of sulfur on the microstructure and surface exchange and diffusion properties of LSCF cathode materials is investigated in the temperature range of 400–900°C on dense bar samples in air using confocal Raman spectroscopy, scanning electron microscopy as well as electrical conductivity relaxation (ECR) methods. Use of dense bar samples will facilitate the observations of microstructure changes and surface property characterizations.[21,22] The results indicate that the deposition of sulfur species on the LSCF surface and formation of S-containing compounds such as $SrSO_4$ and SrS depends strongly on the temperature, and becomes most pronounced at temperatures around 700°C.

Experimental

$La_{0.6}Sr_{0.4}Co_{0.2}Fe_{0.8}O_{3-\delta}$ powders (LSCF, Fuel Cell Materials) were pressed into rectangular bars at 300 MPa, and then fired at 1350°C for 5 h in air to form dense LSCF bar samples. The dimension of the sintered samples is 25 mm × 6.6 mm × 0.62 mm. Sulfur deposition and poisoning experiments were carried out on dense LSCF bar samples by heat-treatment at temperatures from 900 to 400°C in the presence and absence of 20 ppm SO_2 in dry air. The chemical reactivity between La_2O_3, SrO, Co_3O_4 and Fe_2O_3 oxides and sulfur was investigated by calcination of the oxide powders at different temperatures in the presence of 20 ppm SO_2 for 2 h.

XRD (D8 Advance, Bruker, Germany) and confocal laser Raman spectroscopy (WITec GmbH, Ulm Germany) techniques were used to examine the phase formation and composition of oxides and LSCF bar samples. The morphology and microstructure of the bar samples after the heat-treatment at different temperatures in the presence and absence of 20 ppm SO_2 were studied by scanning electron microscopy (SEM) and energy dispersive spectroscopy using a Zesis EVO with 20 keV.

[z]E-mail: s.jiang@curtin.edu.au

The conductivity relaxation profiles of LSCF bar samples were measured by a standard four-probe method using a measurement system consisting of a Digital Multimeter (Keithley 2001) equipped with a computer and a program written using the LABVIEW 8.5 software. Silver wires were used as the leads, which were attached to an Ag electrode using silver paste. The measurements were carried out at temperatures of 700, 800 and 900°C in the presence and absence of 20 ppm SO_2 with oxygen partial pressure changing from 0.05 bar to 0.21 bar. The electrical conductivity data of the bar samples were recorded as a function of exposed time and the experimental data were fitted to the theoretical equations[23] to calculate the oxygen surface exchange coefficients, k_{chem}. However, the samples that were heat treated at temperatures from 600 to 400°C in the presence of 20 ppm SO_2 were not evaluated by ECR due to the very low conductivity value of the LSCF samples at these temperatures. The experimental setup for the ECR measurement and sulfur poisoning arrangement of LSCF bar samples were similar to that used for the boron deposition and poisoning studies.[22]

Results and Discussion

Effect of temperature on the phase and microstructure of LSCF.— Figure 1 is the XRD patterns of LSCF bar samples after heat-treatment in the presence of 20 ppm SO_2 at different temperatures for 48 h. The as-prepared LSCF shows typical XRD patterns associated with rhombohedral perovskite structure (curve a, Fig. 1). After heat-treatment at 800 and 900°C in the presence of 20 ppm SO_2, XRD patterns of LSCF remained the same, suggesting that the main phase is the perovskite structure. However, prominent XRD peaks associated with the formation of $SrSO_4$ phase[24] were observed for the LSCF bar sample treated at 700°C in the presence of 20 ppm SO_2 (curve d, Fig. 1). This indicates the significant reaction between the SO_2 and LSCF bar samples, forming $SrSO_4$ phase. As the heat-treatment temperatures decreased to 600°C–400°C, peaks associated with $SrSO_4$ phase disappear and a distinct peak at 29.5° was detected (curves e,f,g, Fig. 1). The peak at 29.5° has been identified with the formation of SrS phase.[25] The XRD results indicate that the formation of the $SrSO_4$ is most favorable at a temperature of ~700°C, while the formation of SrS occurs at temperatures below 700°C.

Figure 2 is the SEM micrographs of the surface of the LSCF bar samples after heat-treatment in the absence and presence of 20 ppm SO_2 in air at different temperatures for 48 h. As shown previously, the surface of as-prepared LSCF sample is characterized by the dense LSCF grains with smooth surface and the grain size is in the range of 2–5 μm.[22] After heat-treatment in the absence of SO_2, there is a clear formation of isolated small particles on the LSCF surface. For LSCF samples treated at 900°C for 48 h, particles as large as 2 μm are formed (Fig. 2a) and the formation of such particles is most likely due to the segregated cobalt and in particular strontium species.[26] With the decrease in the temperature, the size and number of the segregated particles are reduced significantly. In the case of the LSCF bar sample heat-treated at 400°C for 48 h, the surface is very clean (Fig. 2k), similar to that of as-prepared LSCF sample. These results are in accordance with the surface morphological behavior of LSCF samples after heat-treatment from 600°C to 900°C as reported by Oh et al.[27] and Bucher et al.[28] The significant reduction in the segregated particles indicates that the strontium and/or cobalt segregation on the LSCF electrode is a temperature-activated process.

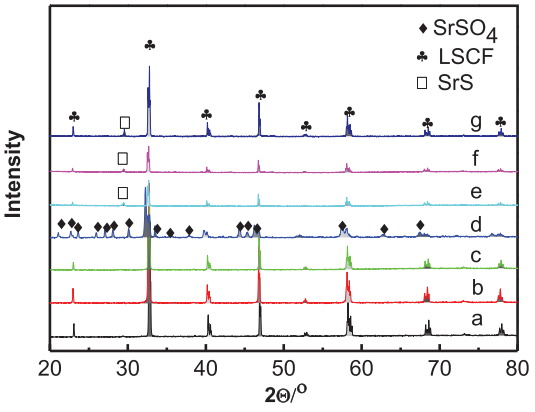

Figure 1. XRD diffraction patterns of as-prepared LSCF and LSCF bar samples after heat-treatment in the presence of 20 ppm SO_2 at different temperatures for 48 h. a) as-prepared, b) 900°C, c) 800°C, d) 700°C, e) 600°C, f) 500°C and g) 400°C.

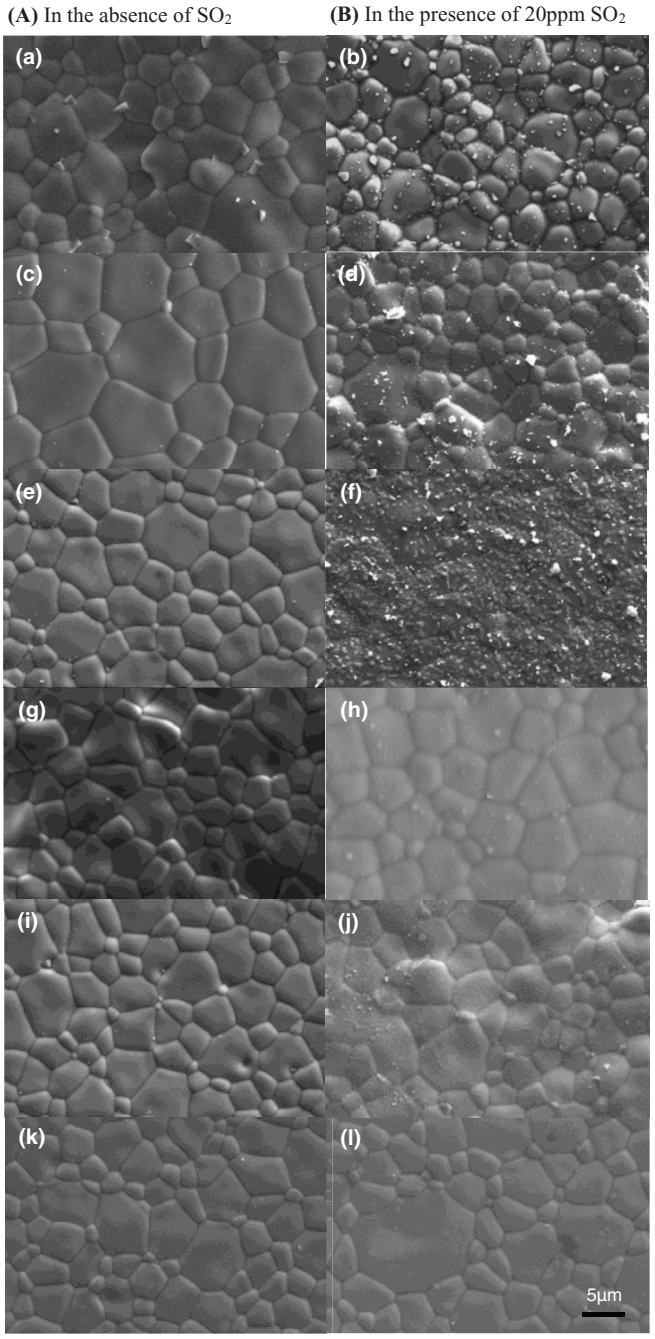

Figure 2. SEM micrographs of LSCF surface after heat-treatment for 48 h (A) in the absence of SO_2 and (B) in the presence of 20 ppm SO_2 at (a,b) 900°C, (c,d) 800°C, (e,f) 700°C, (g,h) 600°C, (i,j) 500°C and (k,l) 400°C. Scale bar applies to all SEM micrographs.

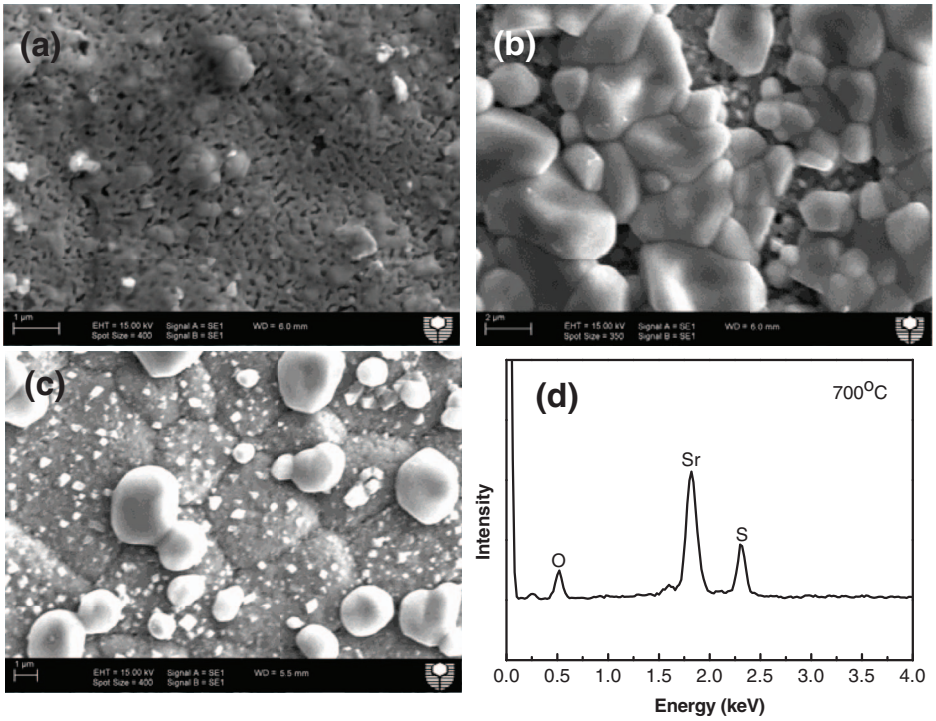

Figure 3. Typical SEM micrographs of LSCF bar samples after heat-treatment in the presence of 20 ppm SO_2 at 700°C for 48 h taken on different samples. EDX of deposited particles is shown in (d).

Very different from that in the absence of SO_2, the size and number of particles formed on the LSCF surface varied significantly with the temperature. For the LSCF sample heat-treated at 900°C in the presence of SO_2 for 48 h, there is a formation of large number of small (∼80 nm) and large (∼700 nm) particles and the formation of the particles appears to be random on both the grain boundaries and the surface of LSCF grains (Fig. 2b). Significant deposition and formation of large and small particles were also observed for the LSCF bar sample after heat-treatment at 800°C (Fig. 2d). However, the most remarkable formation of particles was observed for the LSCF after heat-treatment in the presence of SO_2 at 700°C (Fig. 2f). The surface of LSCF sample is almost completely covered by the particles formed on the surface of LSCF grains. The particles formed on the LSCF surface were most likely strontium sulfate, $SrSO_4$, indicated by the prominent $SrSO_4$ formation as detected by XRD (curve d, Fig. 1). When the temperature decreased to 600°C, the numbers of the particles formed on the LSCF surface decreased substantially with few isolated large particles (400 nm) and numerous fine particles (35 nm) (Fig. 2h). As the temperature is reduced to 400°C, the surface of LSCF bar sample is very clean (Fig. 2l), similar to that in the absence of SO_2 (Fig. 2k). This indicates the significantly reduced activity between the SO_2 and LSCF at temperatures below 700°C.

Figure 3 is the additional SEM micrographs of the deposited particles on different LSCF bar samples after heat-treatment in the presence of 20 ppm SO_2 at 700°C. The deposited particles are characterized by smooth surface without clear crystalline facets (Fig. 3b and 3c). The size of these particles is in the range of 0.5 to 5 μm, much larger than the particles formed at 800 and 900°C. EDX analysis indicates that the deposited particles contain O, Sr and S and the atomic ratio of Sr to S is 1:1 (Fig. 3d), consistent with the $SrSO_4$ phase as identified by XRD.

The phase of the deposited particles on the surface of LSCF bar samples was further investigated using confocal Raman spectroscopy. Figure 4 is the optical microscopy images and Raman spectra of the LSCF surface after heat-treatment at 900 and 800°C in the presence of 20 ppm SO_2 for 48 h. The formation of irregular particles can be clearly observed. $SrSO_4$ has a characteristic Raman adsorption peak at 456, 620 and 1000 cm^{-1}, very close to 460, 620 and 1003 cm^{-1} reported for celestine $SrSO_4$.[24,29] The bright yellow-colored areas in the Raman mapping with wavelength of 1000 cm^{-1} are due to the formation of $SrSO_4$.[30] For the reaction at 900°C, there were formations of large number of small particles along the grain boundaries and based on Raman mapping (Fig. 4A), majority of the particles in the optical microscopy images belong to the $SrSO_4$ phase. As the temperature decreased to 800°C, formation of $SrSO_4$ was also clearly identified (Fig. 4B), similar to that observed for the LSCF bar samples at 900°C. The Raman mapping results evidently show the formation of $SrSO_4$ on the LSCF surface after the heat-treatment in the presence of 20 ppm SO_2 at 800 and 900°C. The detection of $SrSO_4$ phase by the Raman spectroscopy and not by XRD also indicates the high sensitivity of Raman spectroscopy techniques in the study of sulfur poisoning on LSCF electrode materials, particularly in the cases where the quantities of the contaminant phase are very small.

As the temperature decreased to the range of 600–400°C, number of particles deposited on the surface of the LSCF bar samples decreased significantly (Fig. 5). The Raman spectra taken on the surface of LSCF samples after heat-treatment at 600, 500 and 400°C in the presence of 20 ppm SO_2 were similar and no characteristic Raman bands at 456, 620 and 1000 cm^{-1} for $SrSO_4$ were observed (Fig. 5d). No other Raman peaks were observed most likely due to the little Raman activity of near-cubic perovskite phase of LSCF and the face-centered cubic structure of SrS.[25] Both Raman and XRD results indicate that reactivity between the LSCF and SO_2 at temperatures below 700°C to form $SrSO_4$ is very low or negligible. Nevertheless, the detection of SrS by XRD (see Fig. 1) clearly indicates that SrS is the main product of the reaction between LSCF and SO_2 at temperatures below 700°C.

Activity of constituent oxides of LSCF with SO_2.— The reactivity between the constituent oxides of LSCF and SO_2 was studied by heat-treatment of La_2O_3, SrO, Co_3O_4 and Fe_2O_3 oxide powders at 900 to 400°C for 2 h in the presence of 20 ppm SO_2 and the XRD patterns of oxides after the treatment are shown in Fig. 6. In the case of SrO, the major phase is $SrCO_3$ and $Sr(OH)_2$ particularly in the high temperature range 600 to 900°C, probably due to the facile reaction of SrO with CO_2 and moist in the air (Fig. 6b). Distinctive $SrSO_4$ peaks were detected between 900 to 700°C and $SrSO_3$ peaks between 600 to 400°C. However, the amount of $SrSO_4$ and $SrSO_3$ is relatively small as compared to that of $SrCO_3$ and $Sr(OH)_2$. The phases and their relative amount formed for the SrO-SO_2 oxide couples are sum-

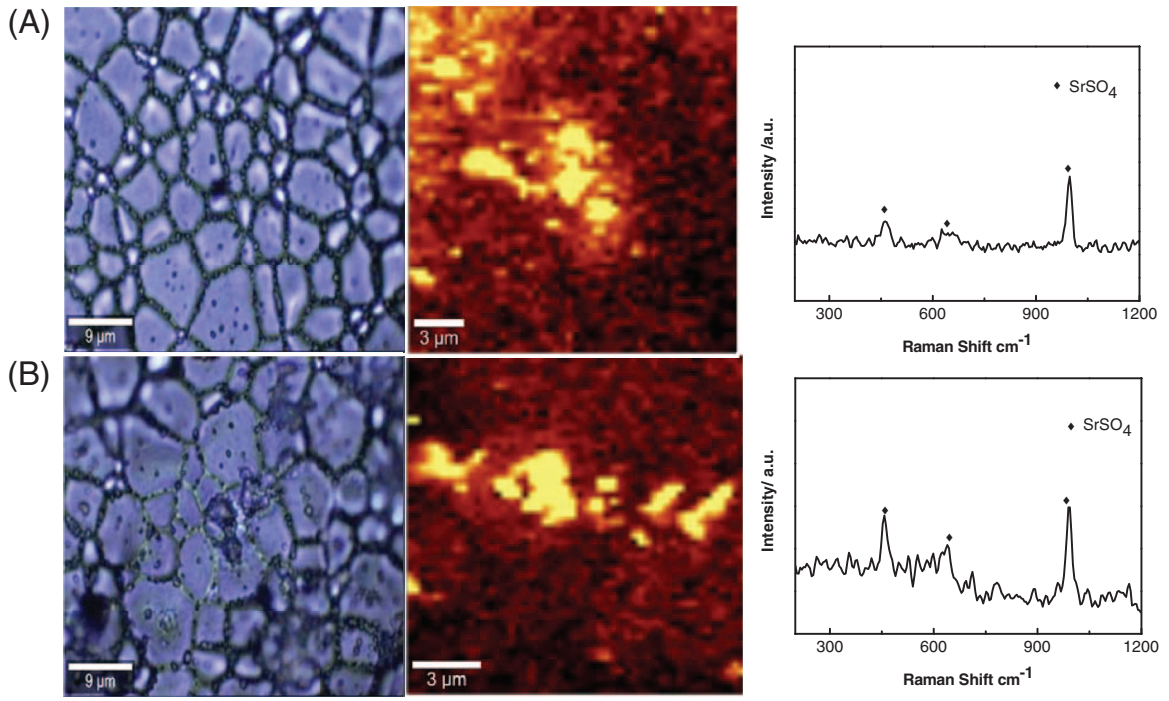

Figure 4. (Left) Optical microscope images of LSCF surface after heat-treatment in the presence of 20 ppm SO_2, (middle) Raman mapping at wavelength of 1000 cm^{-1} corresponding to $SrSO_4$ and (right) Raman spectra from selected areas of LSCF surface. The heat-treatment temperature of the LSCF bar samples was (A) 900°C and (B) 800°C.

marized in Table I. According to the literature, La_2O_3 is reactive with SO_2 to form $La_2(SO_4)_3$ in the temperatures lower than 237°C,[31] while Fe_2O_3 can react with SO_2 in the temperature range of 100 to 750°C but $Fe_2(SO_4)_3$ may decompose above 600°C.[32] Zhao et al.[33] showed that Co_3O_4 reacts with SO_2 at 300°C. However, under the conditions of this study, except the formation of $La(OH)_3$ at 400°C (Fig. 6a), no additional peaks or new phases were observed for the reaction between La_2O_3, Co_3O_4 and Fe_2O_3 oxides and SO_2 (Fig. 6a, 6c, 6d). The results indicate that SrO is most reactive with SO_2, while the activity of La_2O_3, Co_3O_4 and Fe_2O_3 oxides with SO_2 is very low.

Effect of temperature on the oxygen surface exchange coefficient.— Figure 7 is the electrical conductivity relaxation profiles of LSCF samples measured at 900, 800 and 700°C as a function of exposure time in the absence and presence of 20 ppm SO_2. Oxygen partial pressure changes from 0.05 bar to 0.21 bar. In the absence of SO_2,

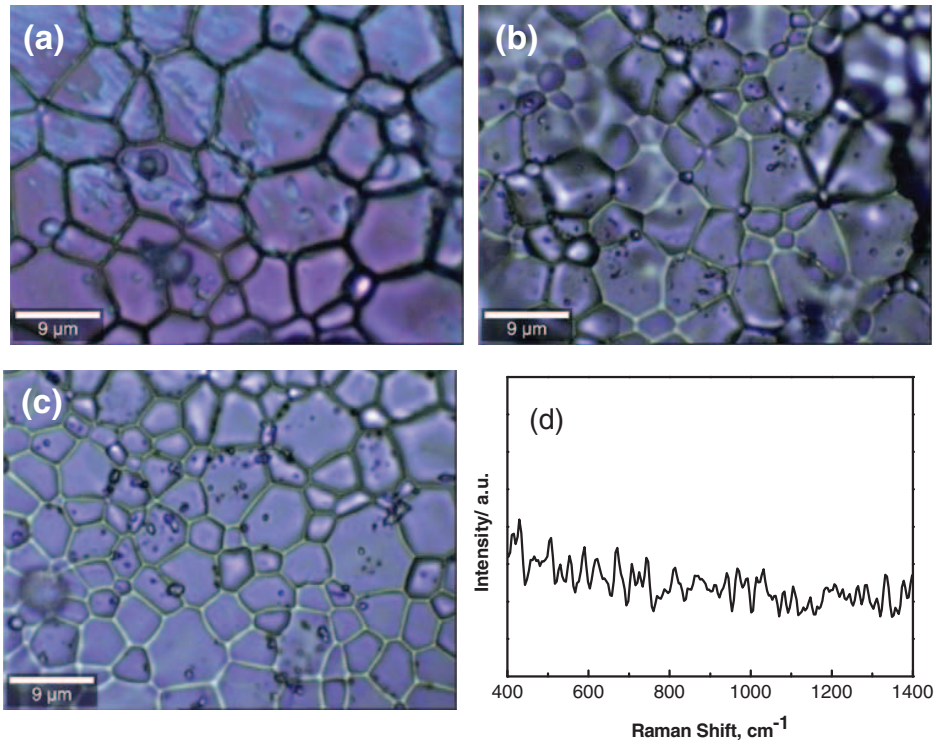

Figure 5. Optical microscope images of LSCF surface after heat-treatment in the presence of 20 ppm SO_2 for 48 h at (a) 600°C, (b) 500°C and (c) 400°C, and (d) typical Raman spectra from selected areas of the LSCF surface.

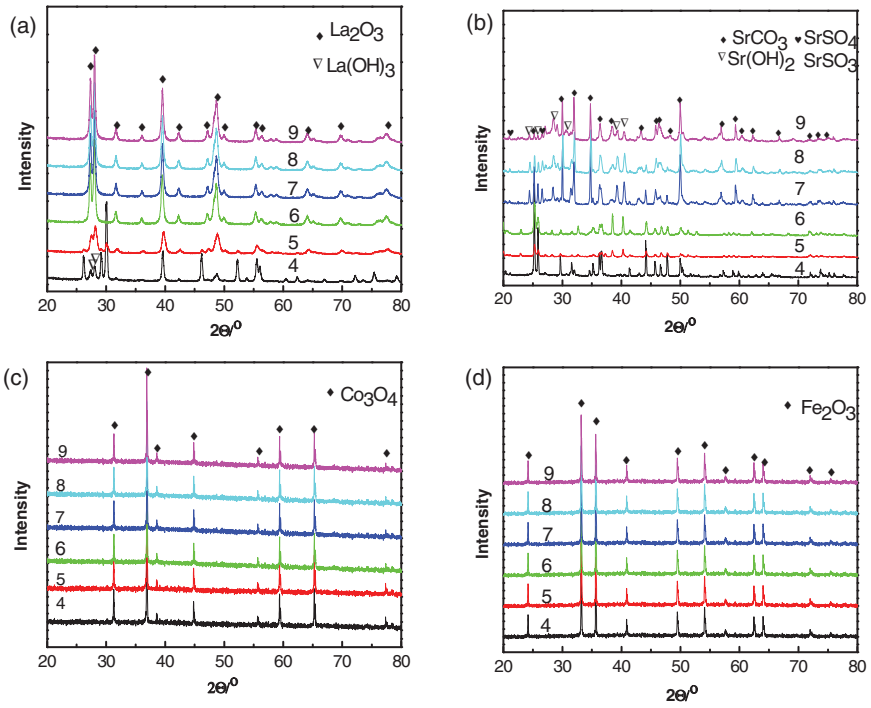

Figure 6. XRD patterns of (a) La_2O_3, (b) SrO, (c) Co_3O_4 and (d) Fe_2O_3 after heat-treatment at different temperatures in the presence of 20 ppm SO_2 for 2 h. The numbers in the figure indicate the temperature: 4–400°C, 5–500°C, 6–600°C, 7–700°C, 8–800°C and 9–900°C.

the initial relaxation time is ~400, 1,000 and 2,000 s, respectively (Fig. 7a–7c). The initial oxygen exchange coefficients, k_{chem} of as-prepared LSCF measured in the absence of SO_2 is 6×10^{-3}, 5×10^{-4} and 2×10^{-4} cm s^{-1} at 900, 800 and 700°C, respectively, and decreased slightly with the heat-treatment time. The small decrease in k_{chem} may be due to the surface segregation of isolated particles on the LSCF surface as shown by SEM analysis (Fig. 2A). However, the relaxation time increases significantly with the exposure time for LSCF samples in the presence of SO_2. For example, the relaxation time increased from 1,500 s to 3,500 s after the heat-treatment in SO_2 from 3 h to 48 h at 900°C (Fig. 7d), while the relaxation time increased from 10,000 s to 30,000 s after the heat-treatment in SO_2 from 3 h to 48 h at 800°C. Similar trend was also observed for the samples heat-treated at 700°C, the relaxation time increased from 8,000 s to 60,000 s (Fig. 7f).

In the presence of 20 ppm SO_2, k_{chem} decreased rather quickly. After the exposure to sulfur for 48 h, the k_{chem} of LSCF at 900°C, 800°C and 700°C is 9×10^{-5}, 8×10^{-6} and 2×10^{-6} cm s^{-1}, respectively, two orders of magnitude lower than that of the as-prepared LSCF. The significant reduction in k_{chem} is clearly related to the sulfur poisoning and formation of $SrSO_4$ on the surface of LSCF cathode materials. As compared to the chromium and boron poisoning, sulfur poisoning is also very significant on the surface exchange properties of the LSCF cathodes. For example, at 800°C, k_{chem} of LSCF after the heat-treatment in the presence of 20 ppm SO_2 for 48 h is 8×10^{-6} cm s^{-1}, significantly lower than 1.0×10^{-4} cm s^{-1} and 6×10^{-5} cm s^{-1} measured after the heat-treatment in the presence of Cr_2O_3 and borosilicate glass for 48 h,[22,34] respectively.

Table I. Reaction products and their relative amount of SrO oxide after the heat-treatment at different temperatures in the presence of 20 ppm SO_2 for 2 h.

	Products			
Temperature,°C	$SrSO_4$	$SrCO_3$	$Sr(OH)_2$	$SrSO_3$
900	L	H	H	
800	L	H	H	
700	L	H	H	
600		L	H	L
500		L	L	L
400		L	L	

*H – high; L – low.

Discussion

The observation of $SrSO_4$ and SrS phases by XRD, SEM and Raman spectroscopy and significant deterioration of k_{chem} of LSCF electrode materials after the heat-treatment in the presence of 20 ppm SO_2 indicate that the presence of sulfur in air can cause the significant sulfur deposition and poisoning of LSCF electrodes for the O_2 reduction reaction, consistent with that reported in the literature.[15,16,18–20,35] The interaction between LSCF and SO_2 leads to the formation of $SrSO_4$ at temperatures ≥700°C and SrS at temperatures below 700°C. Madarasz et al. studied the oxidation behavior of SrS in air and showed that oxidation of SrS starts slowly at 700°C, forming $SrSO_4$.[36] XRD data shows the existence of SrS instead of $SrSO_4$ on the LSCF bar samples after the heat-treatment at 600 to 400°C in the presence of 20 ppm SO_2 and the intensity of the SrS phase increases with the decrease of the temperature (Fig. 1). The disappearance of SrS peaks for the LSCF bar samples heat-treated at temperatures ≥700°C indicates that $SrSO_4$ is more stable than SrS particularly at high temperatures, consistent with that reported by Madarasz et al.[36] In the present study, the sulfur deposition occurs on LSCF dense bar samples under no polarization (i.e., open circuit) conditions. Therefore, the degradation model based on the occupation of SO_2 in the oxide ion vacancies and subsequent formation of SO_3^{2-} and $SrSO_4$ for the sulfur deposition and poisoning[16,20] would not be applicable in this case.

The most significant finding of this study is the unusual behavior of the sulfur deposition on LSCF bar samples as a function of temperature. As shown in Fig. 2A, the Sr segregation of the LSCF decreases with the decrease of temperature, consistent with that reported in the literature.[27,28] Very different from the significant reduction in the surface segregated SrO particles, the sulfur deposition occurred most significantly at temperatures around 700°C (Fig. 2f). The dependency of the Sr segregation and sulfur deposition, i.e., the amount of segregated and sulfur-containing particles formed on the LSCF surface can be semi-quantitatively evaluated, as shown in Fig. 8. In the figure, the degree or magnitude of the surface segregation and sulfur deposition was estimated by measuring the occupied areas of the segregated

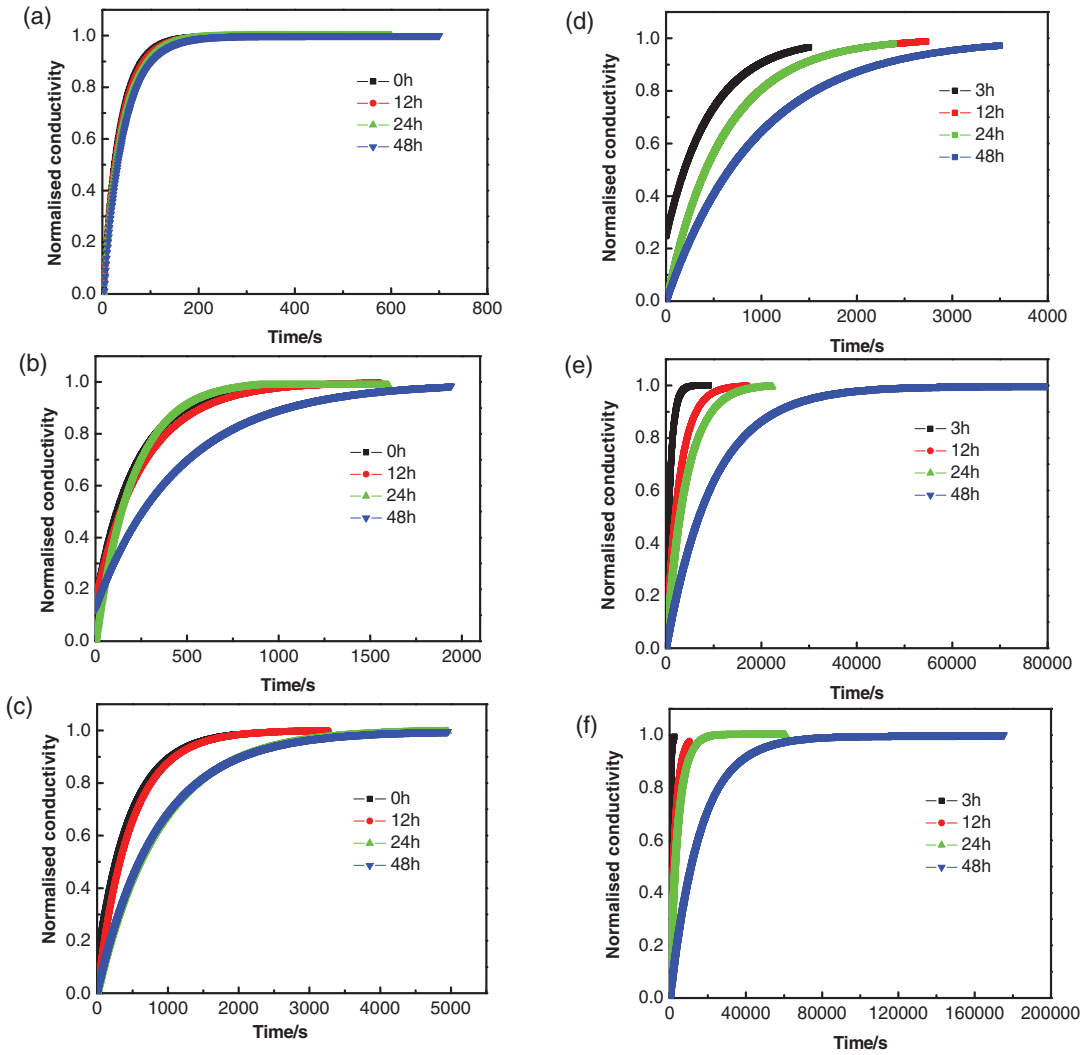

Figure 7. Electrical conductivity relaxation profiles of LSCF bar samples as a function of exposure time in the (a,b,c) absence and (d,e,f) presence of 20 ppm SO_2 at (a,d) 900°C, (b,e) 800°C, and (c,f) 700°C.

particles and the sulfur-containing particles formed on the surface of LSCF bar samples. The occupied areas of particles on the surface were obtained by counting the individual particles per unit area based on the SEM images (similar to that shown in Fig. 2). The areas of the segregated particles on the LSCF surface decrease with the temperature, as expected, however, the areas of sulfur-containing particles show a distinct volcano-shaped curve against the temperature. The areas of the sulfur-containing particles increase with temperature from 900 to 700°C and then decrease dramatically when the temperature decreases from 600 to 400°C.

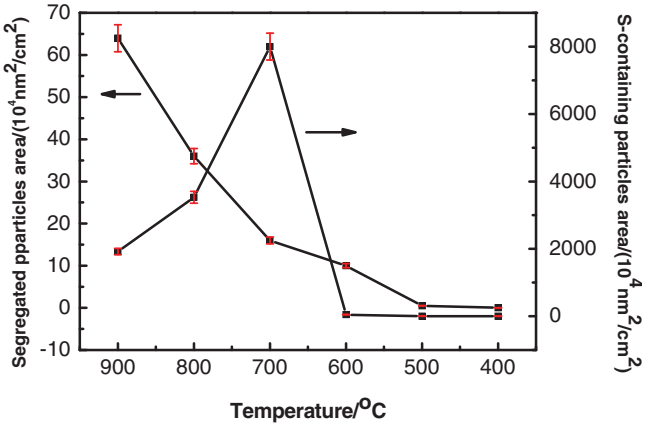

Figure 8. Plots of occupied areas of segregated particles in the absence of SO_2 and sulfur-containing particles in the presence of 20 ppm SO_2, formed on the surface of LSCF bar samples as a function of the heat-treatment temperatures.

In the study of the chromium deposition on LSCF cathode, it is well known that the deposition of Cr species occurs preferentially on the surface of the LSCF cathode and at the LSCF cathode and metallic interconnect interface rather than at the cathode/electrolyte interface, forming primarily $SrCrO_4$.[37–41] The interaction between the SrO and gaseous Cr species would lead to the formation of Sr-Cr-O nuclei on the surface of LSCF and subsequent crystallization and grain growth of $SrCrO_4$ and/or Cr_2O_3 solid phases.[7,38] With the decrease in temperature, both segregated SrO and partial pressure of Cr species decrease significantly, leading to the significant reduction in Cr deposition, as shown recently.[34] The predominant formation of $SrSO_4$ at high temperatures of 900–700°C and SrS at low temperatures of 600–400°C indicates that the segregated SrO also plays an important role in the sulfur deposition and poisoning, similar to that observed in the chromium deposition in the LSCF cathodes.[38]

However, the volcano-type dependency of the sulfur deposition as a function of temperature (Fig. 8) implies that kinetically the nucleation and grain growth for the formation of $SrSO_4$ and SrS phases is a complicated function of temperature. In a recent study of the

effect of SO_2 on the oxygen permeation properties of LSCF hollow fiber membranes, Gao et al also reported that the sulfur content of the LSCF membrane surface layer after the exposure to SO_2 decreased with increase in temperature from 800°C to 1000°C.[42] The decrease in sulfur content indicates the reduced sulfur-containing particles (i.e., $SrSO_4$) with the increase of temperature, consistent with the reduced $SrSO_4$ phase when the temperature increased from 700°C to 900°C in this study. Based on the classical nucleation theory, the nucleation and crystal growth is a competition between the effective diffusion coefficient and energy barrier for the formation and growth of nuclei.[43] For example, in the study of crystal nucleation and growth of NaF in photo-thermo-refractive glass, Dyamant et al.[44] observed the parabolic relationship between the nucleation rates of NaF and temperature with the maximum rate at ∼485°C. $SrSO_4$ phase exhibits an excellent stability from room temperature to 1400°C with a structural transformation at 1158.3°C.[45] Thus, once $SrSO_4$ is formed, the grain growth of the $SrSO_4$ phase would be determined by the kinetics of the reaction between SrO and SO_2. The pronounced formation of $SrSO_4$ at 700°C appears to indicate that the reaction between the SO_2 and segregated SrO depends strongly on the temperature with the highest activity at temperatures close to ∼700°C. This seems to be supported by the observation that at high temperatures of 800 and 900°C the dominant phase formed between SrO and SO_2 is $SrCO_3$ and $Sr(OH)_2$ rather than $SrSO_4$ and $SrSO_3$ (see Fig. 6 and Table I). With the further decrease in temperature to 600°C, the sulfur deposition to form SrS would be limited by segregated SrO due to the substantial reduction in the segregated SrO.

The standard Gibbs free energy, ΔG of possible sulfur compounds of the reaction between LSCF and SO_2 such as $SrSO_4$, $CoSO_4$ and $Fe_2(SO_4)_3$ can be calculated based on the thermodynamic database.[46] For example, at 700°C, the ΔG of $SrSO_4$, $CoSO_4$ and $Fe_2(SO_4)_3$ is –561.74, –171.88 and –57.77 kJ mol^{-1}, respectively. Despite the negative ΔG values, no $CoSO_4$ and $Fe_2(SO_4)_3$ phases were observed by the XRD as well as Raman spectroscopy analysis of the LSCF bar samples after the heat-treatment in the presence of 20 ppm SO_2 under the conditions of the present study. This indicates that kinetically, the reactivity of cobalt and iron oxides with SO_2 is very low. The low activity of cobalt and iron oxides with sulfur is also confirmed by oxide couple study (see Fig. 6) and the reported observation of $SrSO_4$ and $CoFe_2O_4$ and not $CoSO_4$ and $Fe_2(SO_4)_3$ for the sulfur poisoned LSCF cathodes.[16,20]

Conclusions

Sulfur deposition and poisoning mechanism were investigated on dense LSCF bar samples after the heat-treatment in the presence of 20 ppm SO_2 and temperature range of 400 to 900°C, using XRD, SEM, confocal Raman and ECR techniques. SO_2 reacts with LSCF, forming $SrSO_4$ phase at temperatures ≥ 700°C and SrS at temperatures below 700°C. The surface segregation of Sr and/or Co species on the LSCF bar samples decreases significantly with the temperature, however, the sulfur deposition on the LSCF surface shows a distinct volcano-type dependency on the temperature. Sulfur reaction and deposition to form sulfate, $SrSO_4$ is most significant at 700°C. The fundamental reason for such volcano-type sulfur deposition behavior as a function of temperature is not completely understood. However, the results appear to indicate that the reaction between the segregated SrO and SO_2 is most active kinetically at ∼700°C. ECR results indicate that the surface exchange coefficient of LSCF after the exposure to 20 ppm SO_2 at 700, 800 and 900°C for 48 h is 9×10^{-5}, 8×10^{-6} and 2×10^{-6} cm s^{-1}, respectively, which is much lower than 2.8×10^{-4}, 5×10^{-4} and 6×10^{-3} cm s^{-1} of the sample tested in the absence of SO_2. Presence of sulfur in air has a significant detrimental effect on the microstructure and surface exchange coefficient of LSCF electrode materials for the O_2 reduction reaction.

Acknowledgments

The project was supported by Australian Research Council under the Linkage Project funding scheme (project number: LP110200281), Australia. The authors acknowledge the scientific and technical assistance of Dr Thomas Becker of the Department of Chemistry and the facilities of the Curtin University Scanning Probe Microscopy, Department of Chemistry/Nanochemistry Research Institute, the Curtin University Electron Microscope Facility and Curtin X-Ray Laboratory, all of which are partially funded by the University, State and Commonwealth Governments.

References

1. H. Y. Tu and U. Stimming, *J. Power Sources*, **127**, 284 (2004).
2. J. W. Fergus, *International Journal of Hydrogen Energy*, **32**, 3664 (2007).
3. J. A. Schuler, C. Gehrig, Z. Wuillemin, A. J. Schuler, J. Wochele, C. Ludwig, A. Hessler-Wyser, and J. Van Herle, *J. Power Sources*, **196**, 7225 (2011).
4. T. Horita, H. Kishimoto, K. Yamaji, M. E. Brito, Y. P. Xiong, H. Yokokawa, Y. Hori, and I. Miyachi, *J. Power Sources*, **193**, 194 (2009).
5. K. F. Chen, N. Ai, L. Zhao, and S. P. Jiang, *J. Electrochem. Soc.*, **160**, F183 (2013).
6. K. F. Chen, N. Ai, L. Zhao, and S. P. Jiang, *J. Electrochem. Soc.*, **160**, F301 (2013).
7. S. P. Jiang and X. B. Chen, *Int. J. Hydrog. Energy*, **39**, 505 (2014).
8. S. P. Jiang and S. H. Chan, *J. Mater. Sci.*, **39**, 4405 (2004).
9. L. Yang, S. Z. Wang, K. Blinn, M. F. Liu, Z. Liu, Z. Cheng, and M. L. Liu, *Science*, **326**, 126 (2009).
10. K. Sasaki, K. Susuki, A. Iyoshi, M. Uchimura, N. Imamura, H. Kusaba, Y. Teraoka, H. Fuchino, K. Tsujimoto, Y. Uchida, and N. Jingo, *J. Electrochem. Soc.*, **153**, A2023 (2006).
11. Z. Cheng, S. W. Zha, and M. L. Liu, *J. Power Sources*, **172**, 688 (2007).
12. C. M. Grgicak and J. B. Giorgi, *Journal of Physical Chemistry C*, **111**, 15446 (2007).
13. R.-R. Liu, S. Taniguchi, Y. Shiratori, K. Ito, and K. Sasaki, *ECS Transactions*, **35**, 2255 (2011).
14. A. J. Schuler, Z. Wuillemin, A. Hessler-Wyser, and J. Van Herle, *ECS Transactions*, **25**, 2845 (2009).
15. Y. P. Xiong, K. Yamaji, T. Horita, H. Yokokawa, J. Akikusa, H. Eto, and T. Inagaki, *J. Electrochem. Soc.*, **156**, B588 (2009).
16. F. F. Wang, K. Yamaji, D. H. Cho, T. Shimonosono, H. Kishimoto, M. E. Brito, T. Horita, and H. Yokokawa, *J. Electrochem. Soc.*, **158**, B1391 (2011).
17. Z. Cheng, J. H. Wang, Y. M. Choi, L. Yang, M. C. Lin, and M. L. Liu, *Energy & Environmental Science*, **4**, 4380 (2011).
18. E. Bucher, C. Gspan, F. Hofer, and W. Sitte, *Solid State Ionics*, **238**, 15 (2013).
19. J. Xie, Y. W. Ju, and T. Ishihara, *Solid State Ionics*, **249**, 177 (2013).
20. F. Wang, K. Yamaji, D. H. Cho, T. Shimonosono, M. Nishi, H. Kishimoto, M. E. Brito, T. Horita, and H. Yokokawa, *Fuel Cells*, **13**, 520 (2013).
21. K. F. Chen, J. Hyodo, L. Zhao, N. Ai, T. Ishihara, and S. P. Jiang, *J. Electrochem. Soc.*, **160**, F1033 (2013).
22. L. Zhao, J. J. Hyodo, K. F. Chen, N. Ai, S. Amarasinghe, T. Ishihara, and S. P. Jiang, *J. Electrochem. Soc.*, **160**, F682 (2013).
23. J. A. Lane and J. A. Kilner, *Solid State Ionics*, **136**, 997 (2000).
24. M. R. Bissengaliyeva, D. B. Gogol, S. T. Taimassova, N. S. Bekturganov, and A. T. Bort, *Thermochimica Acta*, **565**, 227 (2013).
25. S. Shao, K. Du, K. Huang, L. Cheng, X. Mi, P. Zhou, H. Lin, S. Cui, T. Lin, Z. Ba, and X. Zhang, *Advanced Powder Technology*, **565**, 227 (2006).
26. L. Zhao, J. Drennan, C. Kong, S. Amarasinghe, and S. P. Jiang, *Journal of Materials Chemistry A*, **2**, 11114 (2014).
27. D. Oh, D. Gostovic, and E. D. Wachsman, *Journal of Materials Research*, **27**, 1992 (2012).
28. E. Bucher and W. Sitte, *Solid State Ionics*, **192**, 480 (2011).
29. W. P. Griffith, *Journal of the Chemical Society A: Inorganic, Physical, and Theoretical Chemistry*, 286 (1970).
30. Y.-H. Chen, E. Huang, and S.-C. Yu, *Solid State Communications*, **149**, 2050 (2009).
31. Z. Shichao, *Rare Earth*, **18**, 5 (1997).
32. W. Juxian, *Sulphuric Acid Industry*, **5**, 6 (1992).
33. Z. Xiuge, *Chinese Journal of Catalysis*, **21**, 4 (2000).
34. C. C. Wang, T. Becker, K. F. Chen, L. Zhao, B. Wei, and S. P. Jiang, *Electrochim. Acta*, **139**, 173 (2014).
35. F. F. Wang, K. Yamaji, D. H. Cho, T. Shimonosono, H. Kishimoto, M. E. Brito, T. Horita, and H. Yokokawa, *Solid State Ionics*, **225**, 157 (2012).
36. J. Madarasz, T. Leskela, J. Rautanen, and L. Niinisto, *J. Mater. Chem.*, **6**, 781 (1996).
37. S. P. Simner, M. D. Anderson, G. G. Xia, Z. Yang, L. R. Pederson, and J. W. Stevenson, *J. Electrochem. Soc.*, **152**, A740 (2005).
38. S. P. Jiang, S. Zhang, and Y. D. Zhen, *J. Electrochem. Soc.*, **153**, A127 (2006).
39. M. R. Ardigo, A. Perron, L. Combemale, O. Heintz, G. Caboche, and S. Chevalier, *J. Power Sources*, **196**, 2037 (2011).
40. E. Konysheva, H. Penkalla, E. Wessel, J. Mertens, U. Seeling, L. Singheiser, and K. Hilpert, *J. Electrochem. Soc.*, **153**, A765 (2006).
41. S. P. Jiang, J. P. Zhang, and X. G. Zheng, *J. Eur. Ceram. Soc.*, **22**, 361 (2002).
42. J. Gao, L. P. Li, Z. Yin, J. C. Zhang, S. M. Lu, and X. Y. Tan, *J. Membr. Sci.*, **455**, 341 (2014).
43. W. D. Kinggery, H. K. Bowen, and D. R. Uhlmann, *Introduction to Ceramics*, 2nd Edition, John Wiley & Sons, New york (1976).
44. I. Dyamant, A. S. Abyzov, V. M. Fokin, E. D. Zanotto, J. Lumeau, L. N. Glebova, and L. B. Glebov, *J. Non-Cryst. Solids*, **378**, 115 (2013).
45. Y. F. Li, J. H. Ouyang, and Y. Zhou, *Mater. Chem. Phys.*, **111**, 508 (2008).
46. G. B. Naumov, *Handbook of Thermodynamic Data* (1974).